Thermal resistance across Si-SiGe alloy interface from phonon distribution mismatch

Jinchen Han[1], and Sangyeop Lee[1,2,a)]

[1]Department of Mechanical Engineering and Materials Science, University of Pittsburgh, Pittsburgh, Pennsylvania 15261, USA

[2]Department of Physics and Astronomy, University of Pittsburgh, Pittsburgh, Pennsylvania 15261, USA

a) Authors to whom correspondence should be addressed: sylee@pitt.edu

Abstract:
Interfacial thermal resistance has often been attributed to the mismatch of phonon spectra between two materials and resulting phonon-interface scattering. However, we use the solution of Peierls-Boltzmann transport equation to reveal a substantial nonequilibrium thermal resistance across the interfaces of Si and SiGe alloy at room temperature, despite their nearly identical phonon dispersion and negligible phonon-interface scattering. The Kapitza length of the Si-$Si_{0.99}Ge_{0.01}$ interface is approximately 600 nm of Si. This originates from the mismatch in phonon distribution between Si and SiGe alloy due to their distinct scattering rates. The mismatch is relaxed by phonon scattering over a region of 1 μm around the interface, corresponding to the upper bound of mean free path Λ_x of heat-carrying phonons. The relaxation process leads to the significant entropy generation and increased thermal resistance. Introducing a gradual variation in Ge concentration near the interface markedly reduces thermal resistance when implemented over the 1 μm period. Our finding demonstrates that the interfacial thermal resistance can be significant due to the nonequilibrium phonon distribution, even in the absence of phonon-interface scattering. In addition, among various phonon modes with a wide range of Λ_x, the relaxation of the nonequilibrium is predominantly governed by the phonons with long Λ_x.

Thermal interfaces play a crucial role in governing thermal transport in nano- to micro-scale devices [1-4]. Improving the fundamental understanding of interfacial thermal transport is paramount for designing effective thermal interfaces and manipulating interfacial thermal resistance. Significant progress has been made in understanding phonon-mediated interfacial thermal transport through various theoretical studies [2,3,5-7]. Many of these previous studies focus on the mismatch in phonon spectra between two constituent materials and the atomistic structure at the interface, attributing the interfacial thermal resistance to phonon-interface scattering.

Recently, the nonequilibrium effects have drawn attention for interfacial thermal transport. The nonequilibrium molecular dynamics simulation combined with spectral analysis shows substantially different temperature for each mode in the proximity of interfaces [8,9]. The multi-temperature models, which can be considered simplified forms of the Boltzmann transport equation, also discovered significant energy exchange among phonon modes near Si-Ge interface due to the nonequilibrium phonons [10,11] In our previous studies, we used the kinetic Monte Carlo (MC) solution of the Peierls-Boltzmann transport equation (PBE) and entropy-based resistivity analysis to quantitatively investigate the nonequilibrium thermal resistance, R_{neq}, for the Si-Ge interface [12] and various III-V compound interfaces [13]. Interface-phonon scattering induces distortions in phonon distribution at the interface. As phonon scattering relaxes this distorted (or nonequilibrium) phonon distribution, a substantial amount of entropy is generated, following Boltzmann's H-theorem, contributing to R_{neq} [14]. For many interfaces of III-V compound semiconductors, we observed a positive correlation between R_{neq} and the Debye temperature ratio of the two materials, supporting the connection between interface-phonon scattering and phonon nonequilibrium near the interfaces [13].

However, interface-phonon scattering is not the sole mechanism contributing to R_{neq}. The nonequilibrium resistance can arise from any mechanism causing incoming phonons to exhibit a distribution substantially different from the local equilibrium phonon distribution. In this study, we examine spatially varying phonon scattering rates as a mechanism causing R_{neq}. The interfaces between pure Si and dilute $Si_{1-a}Ge_a$ alloys are chosen as model systems, where the concentration of Ge, 'a', is close to zero. An experimental study of Al-Si and Al-$Si_{0.99}Ge_{0.01}$ interfaces revealed distinct interfacial resistances, explained with the presence of the nonequilibrium thermal resistance [15]. In this work, despite the nearly identical phonon dispersion of dilute SiGe alloys to that of Si, making phonon-interface scattering negligible, the interfacial thermal resistance is shown to be significant due to the strong nonequilibrium effects.

We also demonstrate that R_{neq} can be reduced when the Ge concentration is gradually varied near the interface.

The method used here is elaborated in our previous studies [12,13]. We obtained local phonon distribution by solving the PBE with a kinetic MC method [16]. The Si-SiGe alloy interface is shared by two semi-infinite leads, and self-consistent boundary conditions are implemented to effectively truncate these leads [12]. The interfaces are assumed free from any defects or strain effects. Given the nearly identical phonon dispersion of dilute SiGe alloys compared to pure Si, we use the same harmonic phonon properties and phonon-phonon scattering rate for them and ignore phonon-interface scattering. Therefore, the interfaces between Si and SiGe alloys are invisible to all phonon modes. All other inputs for the PBE, such as phonon dispersion and scattering rates, were calculated using the VASP [17], Phonopy [18], and ShengBTE [19] packages. Further details on the calculation of the phonon properties are given in the Supplementary Materials.

We conducted simulations on five sharp Si-$Si_{1-a}Ge_a$ interfaces, with 'a' taking values of 0.0, 0.001, 0.004, 0.007, and 0.01. In Fig. 1(a), a schematic illustration of a sharp pure-alloy interface is presented. Figure 1(b) compares the mean free paths along the heat flow direction Λ_x for Si and $Si_{0.99}Ge_{0.01}$. While the alloy scattering is weak below 2 THz, it noticeably decreases the Λ_x in the frequency range above 2 THz. As a result, the spectral thermal conductivity for bulk materials, depicted in Fig. 1(c), is strongly impacted, displaying remarkable differences between pure Si and SiGe alloys. For pure Si, phonons across a relatively broad spectrum, up to 5 THz, contribute to thermal transport. However, for $Si_{0.99}Ge_{0.01}$, the modal thermal conductivity above 2 THz is suppressed, and the heat is mostly carried by phonons below 2 THz. The observed mismatch in spectral thermal conductivity between bulk Si and SiGe alloys indicates a substantial difference in the phonon distributions within these bulk samples under a temperature gradient, which is referred to as a bulk distribution or f^{bulk} here.

Considering the substantial difference in f^{bulk} between Si and SiGe alloy far away from the interface, the phonon distribution near the interface is expected to undergo a transition between the two f^{bulk}. The phonon distribution in this transition exhibits more significant deviation from equilibrium compared to the bulk distribution. Consequently, each phonon scattering event generates a larger amount of entropy and thermal resistance compared to bulk materials [12].

Figure 1(d) shows a satisfactory agreement between nonequilibrium resistance values calculated with two distinct methods: (i) subtracting the bulk thermal resistance R_{bulk} from the overall thermal resistance R_{tot}, and (ii) calculating the rate of entropy generation, $\dot{S}$, from

phonon scattering. In the first method, R_{tot} can be found as $\Delta T/q''$, where ΔT and q'' are the temperature difference applied to the computational domain and resulting heat flux, respectively. R_{bulk} is obtained by using the intrinsic bulk thermal conductivity of the constituent material and the lead length. The difference, $R_{\mathrm{tot}}-R_{\mathrm{bulk}}$, encompasses resistance directly from phonon-interface scattering, R_{int}^{0}, and resistance from nonequilibrium phonon distribution, R_{neq}. In this work, R_{int}^{0} is expected to be zero due to the perfect phonon transmission, rendering $R_{\mathrm{tot}}-R_{\mathrm{bulk}}$ representative of R_{neq}. In the second method, we calculate the local nonequilibrium resistivity R'_{neq} from $\dot{S}$ as $R'_{\mathrm{neq}}=(T/q'')^{2}\dot{S}-R'_{\mathrm{bulk}}$, where R'_{bulk} is the bulk resistivity or the reciprocal of intrinsic bulk thermal conductivity. Then, R_{neq} is simply the integral of $R'_{\mathrm{neq}}(x)$ with respect to x. Further details on the calculation of entropy generation rate can be found in our previous studies [12,13].

In Fig. 1(d), the R_{neq} of Si-Si interface, indicated by $a=0$, is negligible because this scenario effectively represents an infinitely large Si sample, and thus R_{tot} should be identical to R_{bulk}. However, the introduction of Ge leads to a notable increase in R_{neq}. For instance, at $a=0.01$, R_{neq} is comparable to the Kapitza length of approximately 600 nm for pure Si. Furthermore, R_{neq} increases almost linearly with the concentration of Ge. This can be attributed to the corresponding linear increase in the alloy scattering rate with the Ge concentration, which causes a larger mismatch of phonon distribution function between bulk Si and SiGe alloy.

Taking advantage of calculating R_{neq} from $\dot{S}$, we can calculate R'_{neq} in real space and obtain R_{neq} for each lead separately by integrating local R'_{neq}. Then, R_{int}^{0} is obtained as $R_{\mathrm{tot}}-R_{\mathrm{bulk}}-R_{\mathrm{neq}}$. The R_{neq} for each lead and R_{int}^{0} are shown in Fig. 1(e). As expected, R_{int}^{0} is negligible in all cases because of the perfect transmission assumed in the simulation. The R_{neq} values of two leads are comparable for all cases.

The comparable R_{neq} for Si and SiGe alloy are further examined with the spatial profiles of R'_{neq} for three Si-$Si_{1-a}Ge_a$ interfaces in Fig. 1(f). The profiles of R'_{neq} are nearly symmetric and the decay lengths of R'_{neq} in Si and SiGe leads are similar, despite the significant difference in Λ_x between Si and $Si_{1-a}Ge_a$ for frequencies above 2 THz shown in Fig. 1(b). This observation suggests the long decay length of nonequilibrium is predominantly determined by the long mean free path of phonon modes with low frequency. Despite the low density-of-states, the contribution of low-frequency modes to thermal transport is substantial as seen in Fig. 1(c) due to their long Λ_x. Below 2 THz, alloy scattering is weak, allowing phonon modes in this frequency range to exhibit similarly long Λ_x in both Si and SiGe alloys. Consequently, in both leads, these phonons are not rapidly relaxed but maintain a significant degree of nonequilibrium over much longer distances

compared to other phonons with shorter Λ_x. Thus, the two leads show similar decay lengths of R'_{neq}.

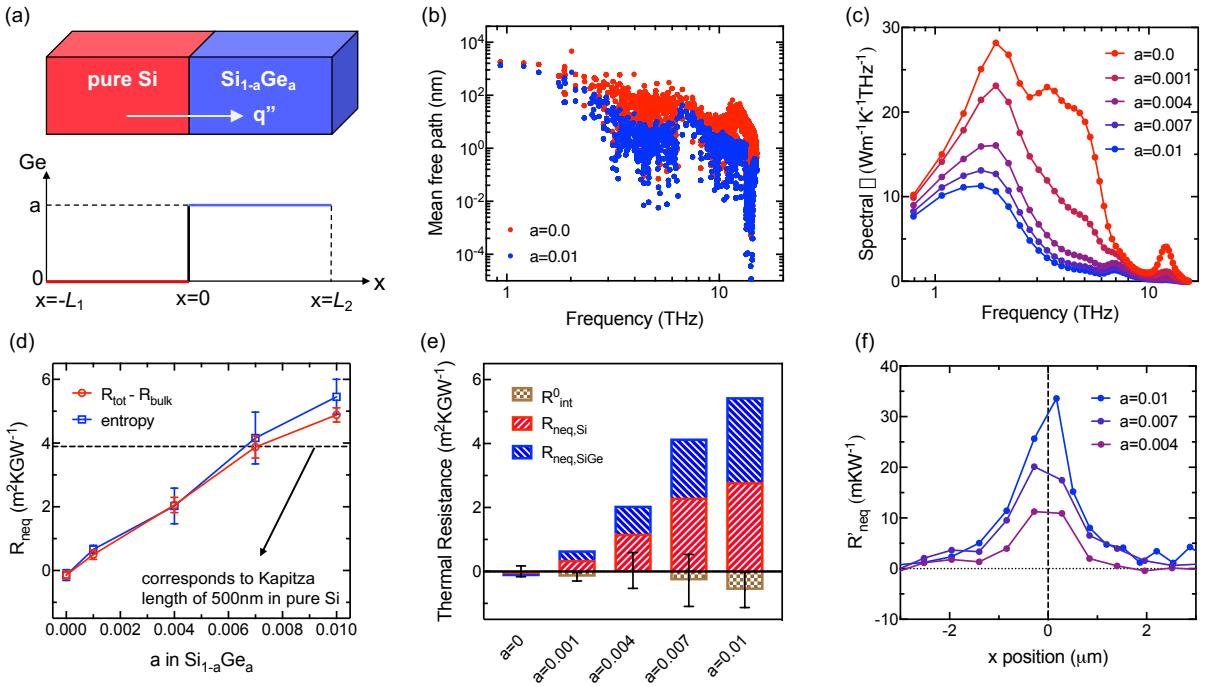

FIG. 1. Sharp Si-$Si_{1-a}Ge_a$ interfaces. (a) Schematic illustration of Si-$Si_{1-a}Ge_a$ interface and Ge concentration variation in space. (b) Modal phonon mean free paths of Si and $Si_{0.99}Ge_{0.01}$ along the heat flow direction. (c) Spectral thermal conductivity with different Ge concentration. (d) Nonequilibrium thermal resistance increasing with the Ge concentration. (e) Nonequilibrium thermal resistance in each lead ($R_{\mathrm{neq,Si}}$ and $R_{\mathrm{neq,SiGe}}$) and the resistance directly from phonon-interface scattering (R^0_{int}). (f) Spatial variation of nonequilibrium thermal resistivity near the interface for three example cases.

We investigate the relationship between R_{neq} and the length scale of system inhomogeneity, which is spatially varying scattering rates in this study. We introduce a transition region located between $x = 0$ and $x = L_{\mathrm{tr}}$ where the Ge concentration linearly increases from zero to 0.01 as schematically illustrated in Fig. 2(a). The methodology is the same as the previous case except that we integrate the bulk resistivity over space in the right lead to calculate R_{bulk} as the Ge concentration varies in the space. We expect that a gradual change of Ge concentration results in less R_{neq} compared to the previous case where the Ge concentration is sharply changed at the interface. To find L_{tr} required to make a noticeable reduction of R_{neq}, we calculate the R_{neq} for four different L_{tr} values of 100, 500, 1000, and 1500 nm.

A clear decrease in R_{neq} as L_{tr} increases is shown in Fig. 2(b). Similar to the sharp interface cases, R_{neq} calculated using two methods show a satisfactory agreement. Additionally, we present R_{neq} for each lead separately in Fig. 2(c) using the entropy calculation. Like the sharp interface cases, R_{neq} of Si and SiGe leads are comparable, and R_{int}^{0} is negligibly small. In Fig. 2(d), we compare R'_{neq} profiles near $x = 0$ for different L_{tr} cases. As L_{tr} increases, the profile of R'_{neq} is broadened with a smaller peak, indicating less significant nonequilibrium phonons.

In Figs. 2(e) and (f), we present the phonon nonequilibrium in the frequency domain at different locations. The figures show the normalized spectral heat flux $\widetilde{q''_{\omega}}$, defined as q''_{ω}/q'', where q''_{ω} is a spectral heat flux, for the sharp interface and the gradual interface with L_{tr}=1500 nm. The dots are actual $\widetilde{q''_{\omega}}$ from the MC solution of PBE. The solid lines are $\widetilde{q''_{\omega}}$ of bulk Si and SiGe alloy with a Ge concentration corresponding to the location denoted in the legend. The deviations of points from the solid lines represent the degree of phonon nonequilibrium induced by the interface.

Comparing Figs. 2(e) and (f), the interface with a transition region in Fig. 2(f) exhibits a more gradual change in $\widetilde{q''_{\omega}}$ with the location, supporting the observed lower nonequilibrium resistance in Figs. 2(b) and (c). Below we discuss $\widetilde{q''_{\omega}}$ in alloy and pure Si leads separately.

In the alloy region (x>0), depicted in blue in Figs. 2(e-f), the degree of nonequilibrium is markedly diminished. Above 2 THz, the $\widetilde{q''_{\omega}}$ closely aligns with the bulk $\widetilde{q''_{\omega}}$, irrespective of the spatial variation of Ge concentration – be it sharp or gradual. This is attributed to the sufficiently short Λ_x in this spectrum facilitating rapid relaxation of the nonequilibrium distribution to f^{bulk}. On the contrary, below 2THz, the gradual interface shows a notably reduced degree of nonequilibrium. This reduction is mainly because of the gradual change in bulk $\widetilde{q''_{\omega}}$ across the transition region. For instance, the solid line at x=510 nm in Fig. 2(f) mitigates the significant change in $\widetilde{q''_{\omega}}$ from $x \to -\infty$ to $x \to +\infty$. Nonetheless, an L_{tr} of 1500 nm is insufficient to suppress the nonequilibrium below 2 THz to a similar degree as above 2 THz range. This highlights spatially persistent nonequilibrium due to the long Λ_x of low-frequency phonons.

The gradually varying Ge concentration also helps to reduce the nonequilibrium in pure Si lead for the entire phonon spectrum. A noticeable difference from the SiGe alloy is the phonon nonequilibrium above 2 THz. While the nonequilibrium is small above 2 THz in the SiGe alloy, the phonons in Si lead exhibit noticeable nonequilibrium in this frequency range. This disparity is attributed to the significantly weaker phonon scattering above 2 THz in Si compared to SiGe alloy, due to the absence of alloy scattering as shown in Fig. 1(b). In Fig. 2(f), although the gradual

variation of Ge concentration reduces the nonequilibrium to some extent in the entire spectrum, phonons below 2 THz still exhibit noticeable nonequilibrium, similar to the SiGe alloy lead.

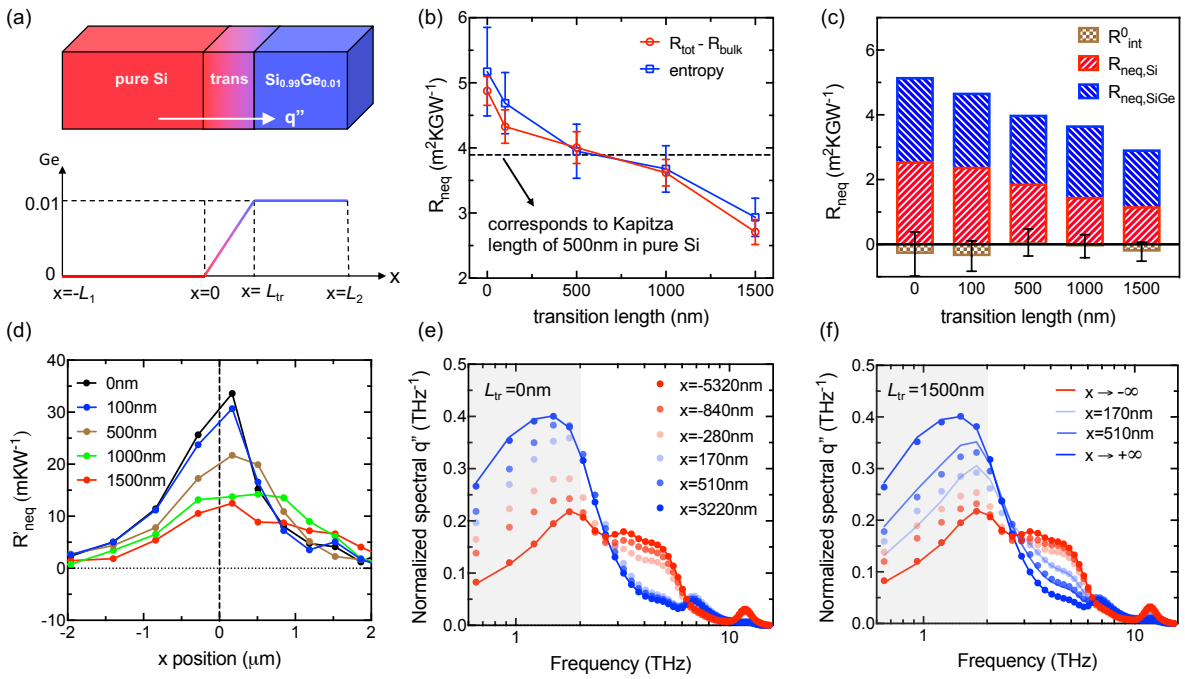

FIG. 2. Si-$Si_{0.99}Ge_{0.01}$ interfaces with a transition region where Ge concentration gradually changes. (a) Schematic illustration of Si-$Si_{0.99}Ge_{0.01}$ interface with linearly increasing Ge concentration in space. (b) Nonequilibrium thermal resistance for different transition region lengths. (c) Decomposed nonequilibrium thermal resistance. The blue bar includes both the transition region and $Si_{0.99}Ge_{0.01}$ lead. (d) Nonequilibrium thermal resistivity near $x = 0$. (e-f) Normalized spectral heat flux $\widetilde{q''_\omega}$ at different locations for the sharp Si-$Si_{0.99}Ge_{0.01}$ interface and the interface with L_{tr} of 1500 nm. The dots represent actual $\widetilde{q''_\omega}$. The solid lines represent $\widetilde{q''_\omega}$ of bulk sample with corresponding Ge concentration. For example, red and blue solid lines denoted as $x \to +\infty$ and $x \to -\infty$ are $\widetilde{q''_\omega}$ in bulk Si and $Si_{0.99}Ge_{0.01}$ samples.

In summary, we demonstrated that the thermal resistance across the Si-SiGe alloy interface is significant and linearly increases with Ge concentration, even in the absence of phonon-interface scattering. For the Si-$Si_{0.99}Ge_{0.01}$ interface, the Kapitza length is approximately 600 nm of pure Si. The significant interfacial thermal resistance arises from the nonequilibrium distribution of phonons. Far from the interface, phonon distributions in Si and SiGe alloy leads exhibit a substantial difference because of the alloy scattering in SiGe alloy. The mismatch of phonon distribution is relaxed near the interface through phonon scattering, generating the entropy and thus thermal resistance. Gradually changing the Ge concentration between pure Si

and $Si_{0.99}Ge_{0.01}$ reduces the nonequilibrium resistance as it suppresses the strong nonequilibrium. When the concentration of Ge is linearly varied from 0 to 0.01 over 1 μm, the interfacial thermal resistance is reduced to approximately half. All simulation results indicate that the length scale of nonequilibrium effects is mainly determined by the upper bound of Λ_x of heat-carrying phonons. Because alloy scattering does not significantly decrease the long Λ_x of low-frequency phonons, Si and SiGe alloy exhibit similar decay lengths for the R'_{neq}. To achieve a noticeable reduction of R_{neq}, the Ge concentration needs to be varied over the length scale comparable to the upper limit of Λ_x of heat-carrying phonons.

Supplementary Material

Details of phonon scattering rate calculation and the scattering rates for different Ge concentrations

Acknowledgement

We thank Richard Wilson for helpful discussions. We acknowledge support from National Science Foundation (Award No. 1943807). This research was also supported in part by the University of Pittsburgh Center for Research Computing, RRID:SCR_022735, through the resources provided. Specifically, this work used the H2P cluster, which is supported by NSF award number OAC-2117681.

References

[1] T. Feng, H. Zhou, Z. Cheng, L. S. Larkin, and M. R. Neupane, ACS Applied Materials & Interfaces **15**, 29655 (2023).
[2] J. Chen, X. Xu, J. Zhou, and B. Li, Reviews of Modern Physics **94**, 025002 (2022).
[3] A. Giri and P. E. Hopkins, Advanced Functional Materials **30**, 1903857 (2020).
[4] C. Monachon, L. Weber, and C. Dames, Annual Review of Materials Research **46**, 433 (2016).
[5] H. Zhou, Z.-Y. Ong, G. Zhang, and Y.-W. Zhang, Nanoscale **14**, 9209 (2022).
[6] M. Hu and Z. Yang, Phys Chem Chem Phys **23**, 1785 (2021).
[7] P. Zhang, P. Yuan, X. Jiang, S. Zhai, J. Zeng, Y. Xian, H. Qin, and D. Yang, Small **14**, 1702769 (2018).
[8] T. Feng, Y. Zhong, J. Shi, and X. Ruan, Physical Review B **99**, 045301 (2019).
[9] T. Feng, W. Yao, Z. Wang, J. Shi, C. Li, B. Cao, and X. Ruan, Physical Review B **95**, 195202 (2017).
[10] Z. Lu, J. Shi, and X. Ruan, Journal of Applied Physics **125**, 085107 (2019).
[11] J. Maassen and V. Askarpour, APL Materials **7**, 013203 (2019).
[12] X. Li, J. Han, and S. Lee, Materials Today Physics **34**, 101063 (2023).
[13] J. Han and S. Lee, Physical Review Materials **8**, 014604 (2024).
[14] S. Lee, X. Li, and R. Guo, Nanoscale and Microscale Thermophysical Engineering **23**, 247 (2019).
[15] R. B. Wilson and D. G. Cahill, Nature Communications **5**, 5075 (2014).
[16] J.-P. M. Péraud and N. G. Hadjiconstantinou, Applied Physics Letters **101**, 153114 (2012).
[17] J. Hafner, Journal of Computational Chemistry **29**, 2044 (2008).
[18] A. Togo and I. Tanaka, Scripta Materialia **108**, 1 (2015).
[19] W. Li, J. Carrete, N. A. Katcho, and N. Mingo, Computer Physics Communications **185**, 1747 (2014).